

The Kaidun meteorite: Clasts of alkaline-rich fractionated materials

Andrei V. IVANOV,^{1*} Nataliya N. KONONKOVA,¹ S. Vincent YANG,² and Michael E. ZOLENSKY³

¹Vernadsky Institute of Geochemistry and Analytical Chemistry, Moscow 117975, Russia

²Lockheed Engineering and Science Company, Houston, Texas 77258, USA

³SN2, NASA Johnson Space Center, Houston, Texas 77058, USA

*Corresponding author. E-mail: andrei_ivanov@geokhi.ru

(Received 9 April 2002; revision accepted 11 November 2002)

Abstract—Clasts of alkaline (the second find in meteorites) and subalkaline rocks were found in the Kaidun meteorite. One of them (#d4A) is a large crystal of albite with inclusions of fluorapatite, arfvedsonite, aenigmatite, and wilkinsonite. The two latter minerals were previously unknown in meteorites. Another clast (#d[3–5]D) has a melt crystallization texture of mainly feldspar (oligoclase) composition and contains relict grains of both high-Ca and low-Ca pyroxene and fluorapatite. The mineralogical characteristics of these clasts suggest a genetic relationship and an origin from the same parent body. The textural and mineralogical characteristics of the clasts indicate origin by extensive igneous differentiation. Such processes most likely took place in a rather large differentiated body. The material of clast #d(3–5)D is similar in some mineralogical respects to basaltic shergottites.

INTRODUCTION

The Kaidun meteorite is an extremely unusual heterogeneous breccia. Kaidun, as a whole, is classified as a CR2 carbonaceous chondrite (Ivanov 1989; Ivanov et al. 1987; Clayton et al. 1994) and contains numerous inclusions of different types. These include CI type (Ivanov 1989; Ivanov et al. 1987; Clayton et al. 1994), an unusual CM1 lithology containing many mineralogical features not previously reported in meteorites (Zolensky et al. 1996), and fragments of different enstatite chondrites. An EL3 chondrite fragment was the first such material found in any meteorite (Ivanov and Ulyanov 1985). An EH fragment contains many products of nebular condensation including the unusual compound Na₂S₂ (Ivanov et al. 1996), and another one shows evidence for both nebular and parent body aqueous alteration of metal (Ivanov et al. 1998). We found a geode of Fe, Ni metal crystals which appears to have formed as a result of carbonyl transportation (Ivanov et al. 1988). Along with the forementioned sodium sulfide Na₂S₂, we discovered an unusual Fe, Cr sulfide with stoichiometry close to daubreeelite but with a constantly low analytical sum and strong optical anisotropy (Ivanov 1989; Ivanov et al. 1996, 1998), and the mineral florenskyite FeTiP, which is the first phosphide of a lithophilic element found in nature (Ivanov et al. 2000b).

Kaidun is a unique meteorite that has no known analogues. Undoubtedly, the key to understanding the origin

and nature of this enigmatic meteorite lies in studying its different components. In this paper, we describe the results of our investigation of two clasts, #d(3–5)D and #d4A, that show evidence of formation by igneous differentiation, and that appear to be genetically related.

EXPERIMENTAL PROCEDURES

We studied doubly-polished thin sections of the Kaidun fragments #d4A and #d(3–5)D. A petrographic and mineralogical study was performed by traditional optical microscopy and scanning electron microscopy. We used a JEOL JSM-35CF at the Johnson Space Center (JSC), Houston, Texas, and a CAMSCAN at Moscow State University. Both machines were operated at 15 kV to obtain backscattered electron images.

We determined the chemical composition of matrix and mineral phases using a Cameca Camebax-Microbeam electron microprobe at the Vernadsky Institute in Moscow and Cameca SX 100 at JSC. In most cases, the analyses were carried out at 30 nA and accelerating voltage of 15 kV. For mineral phases with higher volatile composition, we performed the analyses in a raster scanning mode with a line spacing of 2 μm, a 10 nA beam current, and a 15 kV accelerating voltage. A raster scanning mode with a line spacing of 50 μm also was used to obtain the matrix composition of the #d(3–5)D clast. Natural minerals and

synthetic compounds were used as standards and ZAF-corrections were applied.

The bulk chemical composition of clast #d(3–5)D was calculated using matrix and mineral composition data and the results of a quantitative mass balance mineralogical calculation.

DESCRIPTION AND TEXTURE OF CLASTS

Clast #d4(3–5)D

Clast #d(3–5)D is present in 3 polished thin sections—#d3, #d4, and #d5—obtained by sequential cutting of a fragment of Kaidun. According to a predefined system, we named the clast #d(3–5)D and its thin sections #d3D, #d4D, and #d5D. The thin sections of this clast are irregular and are 1.9×2.1 , 2.6×3.0 , and 2.2×4.0 mm in size, respectively. The clast's texture, mineral assemblage, and mineral compositions are essentially identical in all 3 sections (Fig. 1).

The clast's overall texture is defined by an ophitic main mass speckled with large apatite and pyroxene grains. Section #d3D contains 3 grains each of pyroxene and apatite, #d4D contains 5 pyroxene grains and 2 apatite grains, and #d5D contains 1 pyroxene grain. We note that #d3D is the first thin section to contain this clast. It appears to contain the edge of the clast. At its edge, #d3D contains a rounded, amoebae-shaped piece of Kaidun's carbonaceous matrix in contact with the clast material, which, at this site, is a uniform, crystal-free glassy mass (Fig. 2).

The large pyroxene grains have irregular shapes ranging from equant to elongate and are 400×300 to 140×80 μm in size. The pyroxene grains are characteristically rounded. Eight of the 9 pyroxene grains found in the thin sections are high-Ca and one (190×80 μm) is low-Ca.

In section #d3D, the apatite grains are 70 – 120 μm in size and are equant to slightly elongate. The apatite grains show clear faces and corners, and one of the grains is a regular hexagon. In section #d4D, an apatite grain ~ 100 μm across

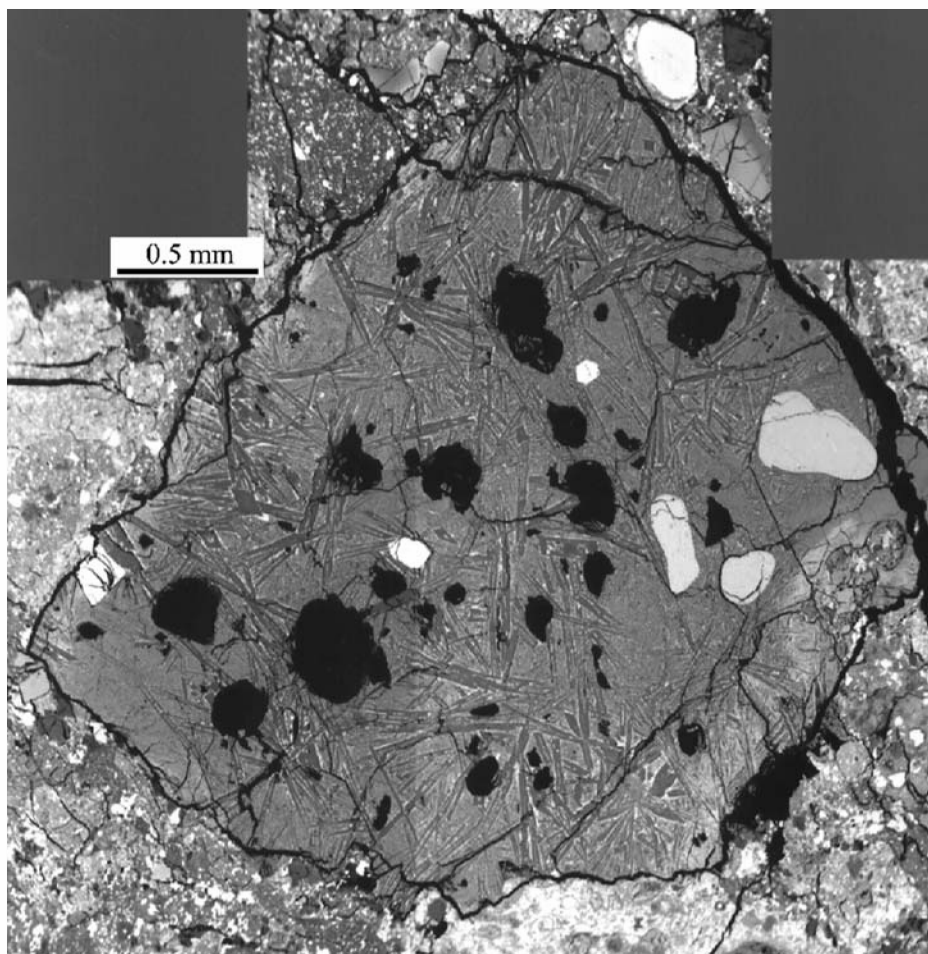


Fig. 1. Backscattered electron image of Kaidun fragment #d(3–5)D, section #d3D. The clast's overall texture is defined by an ophitic main mass speckled with large apatite and pyroxene grains. The dark irregular areas are holes, the large light-gray grains with roundish outlines are high-Ca pyroxenes, and the small white grains are apatite. The apatite grain at the center is a regular hexagon with clear faces and corners. The scale bar is 0.5 mm.

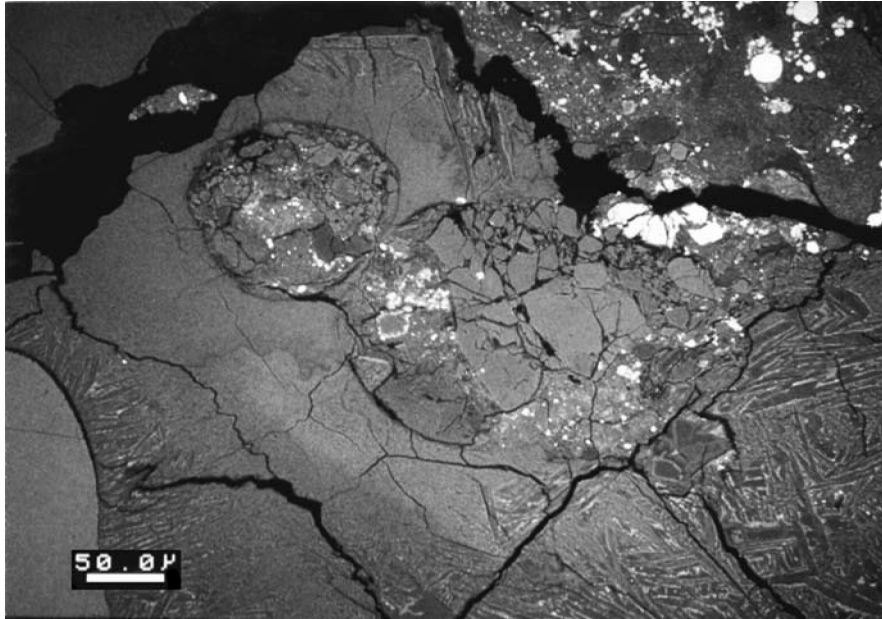


Fig. 2. Backscattered electron image of a piece of carbonaceous matrix at the edge of fragment #d(3–5)D, section #d3D. The rounded contact between the body of the clast and the carbonaceous inclusion indicate that the material of the clast was liquid during formation of the contact. The scale bar is 50 μm .

also has a hexagonal shape but with rounded corners. One fragment of a second apatite grain in section #d4D is located at the very edge of the clast.

The main mass of clast #d(3–5)D consists of crystals of plagioclase submerged in a finely crystalline mass of complex composition (Fig. 3). The finely crystalline mass becomes glassy toward the edges of the clast. The plagioclase crystals are commonly lath-shaped, $\sim 400 \times 40 \mu\text{m}$ in size, and are skeletal to rectangular. Some laths are curved. Plagioclase laths commonly intergrow in various shapes, including star-shaped. Regular plagioclase rhombuses with a long axis up to 130 μm are common. All types of plagioclase crystals are usually surrounded by thin pyroxene crystals. Inclusions of composition similar to pyroxene—and usually rich in phosphorus—are common in the inner areas of the plagioclase crystals. Potassium-rich grains with anorthoclase composition are ubiquitous in the matrix. No opaque phases were found in the clast. Clast #d(3–5)D contains voids ranging from a few tens of microns up to ~ 0.5 mm in size. The large voids have complex, irregular shapes. In many cases, the voids interrupt or completely crosscut plagioclase laths. We did not note any patterns in the locations of the voids. Small voids $< \sim 100 \mu\text{m}$ occur preferentially but not exclusively in the finely crystalline areas of the main mass of the clast. The small voids often have a rounded or elongated almond shape. Sometimes these elongated voids aligned.

The walls of the small voids, in many cases, are covered with a thin mineralized layer having a typical thickness of $< 10 \mu\text{m}$, but varying up to 18 μm . The varying thickness may be due to the plane of the section not being parallel to the voids'

diameter. The layering has two structural types—in some cases the layer is made from a brushy mass of thin needle-shaped crystals (Fig. 4), and in others, it is colloform. Layers with a fine crystal structure occur primarily near the edges of the clast and are found primarily in section #d3D. Both types of coating commonly occur in a single void in which the colloform coating overlaps and covers the crystalline coating. In these cases, the boundary between the coatings is usually irregular and indistinct. We found a few plagioclase laths interrupted by voids with coated walls.

Clast #d4A

In thin section #d4, about 4 mm from #d4D, we found a twinned crystal of plagioclase (clast #d4A) 1.2×0.7 mm in size (Fig 5). The crystal contains irregular 30–40 micron inclusions of apatite. The crystal is intersected by a fractured zone containing 3–8 micron calcium phosphate grains.

The central part of an albite crystal contains an elongate $150 \times 50 \mu\text{m}$ polymineralic inclusion (Fig. 6). The inclusion's main phase is aenigmatite in the form of an elongated, partially fragmented grain $85 \times 20 \mu\text{m}$ in size and several adjacent small grains ($< 10 \mu\text{m}$). Small, rounded phosphate inclusions are present in the middle of the largest aenigmatite grain. Aenigmatite also occurs intergrown with apatite.

Among the small aenigmatite grains are several small ($< 5 \mu\text{m}$) grains of wilkinsonite, which is a mineral of the aenigmatite group (Fig. 7). In one case, wilkinsonite occurs as thin exsolution-like inclusions within an aenigmatite grain. This is the first time aenigmatite and wilkinsonite have been

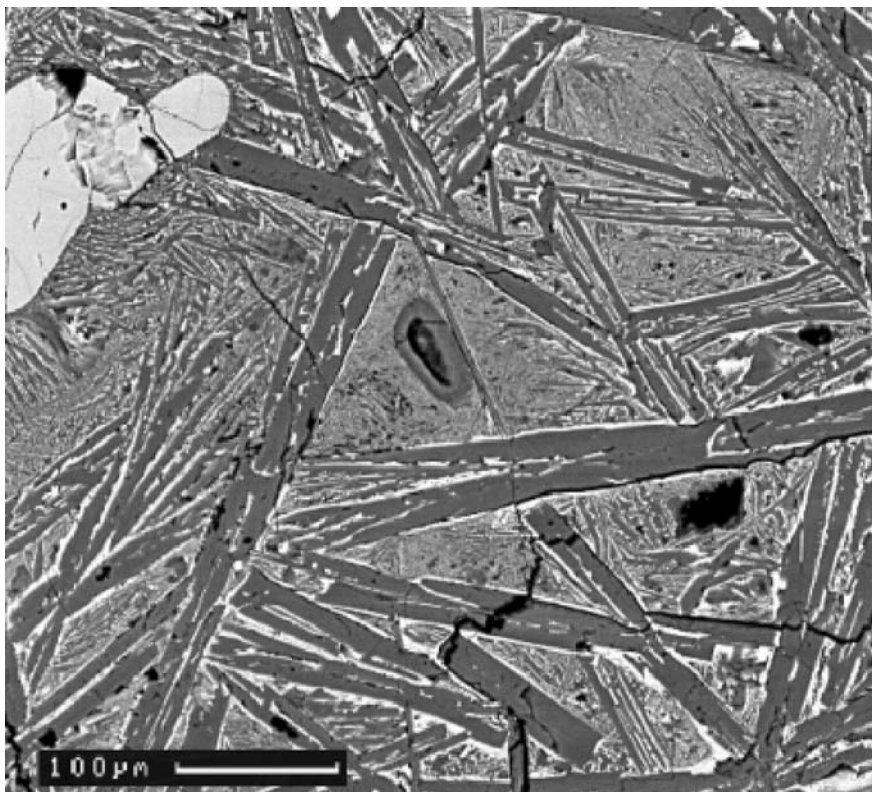


Fig. 3. Backscattered electron image of the texture of the main part of fragment #d(3–5)D, section #d4D. The elongate lath-shaped plagioclase crystals are submerged in a finely crystalline mass. At the center is a void with a colloform coating. Part of a high-Ca pyroxene grain is at the upper left. The scale bar is 100 μm .

found in meteorites and only the second time wilkinsonite has been found in nature (Duggan 1990).

In this inclusion, we also identified rounded grains of arfvedsonite about 15 μm in diameter. On one side, the grains of aenigmatite are coated with Fe and Mg phyllosilicates containing calcium phosphate inclusions.

CHEMICAL COMPOSITION OF THE COMPONENTS

Clast #d(3–5)D

Table 1 shows the chemical composition of the components of clast #d(3–5)D.

In all 3 sections of clast #d(3–5)D, the large grains of high-Ca pyroxene contain nearly constant major element compositions (augite $\text{En}_{42.4}\text{Fs}_{21.6}\text{Wo}_{36.0}$). The variations of the minor element compositions in these pyroxene grains are typical for augite. The only low-Ca pyroxene grain we found has a pigeonite composition of $\text{En}_{47.2}\text{Fs}_{42.9}\text{Wo}_{9.9}$. Chemical zoning is absent in these crystals. Apatite grains in clast #d(3–5)D have a fairly constant chlorfluorapatite composition (Table 1).

Matrix plagioclase of all morphological types is usually characterized by a high content of foreign components such as TiO_2 , FeO, MgO, P_2O_5 . Table 1 shows only the purest

compositions. Plagioclase (average $\text{An}_{21.8}\text{Ab}_{76.7}\text{Or}_{1.5}$) varies widely in composition ($\text{An}_{16.0-34.5}\text{Ab}_{64.6-82.1}\text{Or}_{0.8-1.2}$). Zoning is absent in plagioclase crystals.

Wide variations in composition also were noted in the fine subcalcic augite crystals of the matrix ($\text{En}_{27.9-40.6}\text{Fs}_{36.3-53.7}\text{Wo}_{14.7-26.7}$). Matrix pyroxenes are characterized by high phosphorus, which is not typical of pyroxenes. Some portions of the matrix had a potassium-rich anorthoclase composition. In these areas, the potassium content reached 2.5 wt%.

A peculiarity of the chemical composition of the matrix of clast #d(3–5)D is the extremely high and variable content of alkaline elements and phosphorus. For example, the average and maximum K_2O content in the matrix substantially exceed those in the plagioclase crystals. In normalized composition, the matrix of the clast is more than 83.5 vol% plagioclase ($\text{Ab}_{82.2}\text{An}_{14.2}\text{Or}_{3.6}$), 9 vol% pyroxene, and 5.8 vol% olivine.

The collomorphic coatings covering the walls of the small voids have a consistently low analytical sum (85–92 wt%) and, based upon the composition (Table 2), consist of phyllosilicates of the chlorite-serpentine group. The composition of these coatings is substantially different in different voids but fairly constant within a given void. We did not observe chemical zoning in these coatings.

A characteristic of the composition of the finely

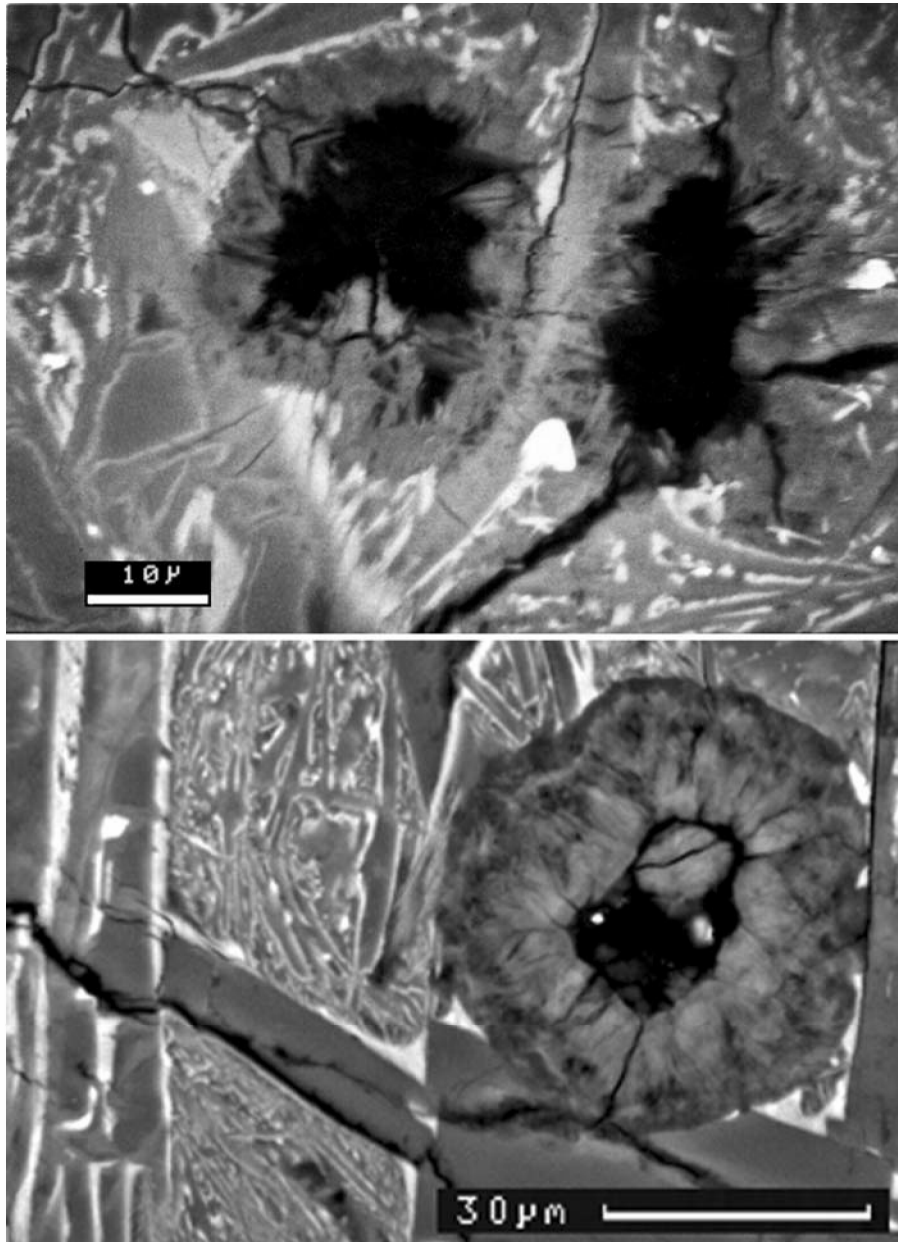


Fig. 4. Backscattered electron images of voids with coatings of different structural types in fragment #d(3–5)D, section #d4D: two voids with crystalline coating (above, scale bar 10 μm) and a void with colloform coating (below, scale bar 30 μm). The coatings also differ widely in chemical composition (see Table 2).

crystalline coatings within voids is a high content of MgO , FeO , and Al_2O_3 , with a very low SiO_2 content and the nearly total lack of almost all other analyzed components. The analytic sums are also consistently low (Table 2, Fig.8). The crystalline coating is very thin and its boundary with the collomorphic coating is irregular. As a result, microprobe analyses of the crystalline coating inevitably pick up a contribution from the collomorphic coating because the microprobe spot size (~3 microns) is larger than the thickness of the crystalline coating. Specifically, we believe that our SiO_2

measurements for the finely crystalline coating may include some contribution of SiO_2 from the collomorphic coating.

We have performed additional calculations to attempt to correct for this effect. As shown in Table 2, we have subtracted the suspected contribution of the collomorphic coating from the measured composition of the finely crystalline coating. The resulting calculated compositions are well-approximated by the formula $(\text{Mg}, \text{Fe}, \text{Mn})_5\text{Al}_2\text{O}_8 \cdot n\text{H}_2\text{O}$. Both coating types contain sulfur, which was not observed in the other components of clast #d(3–5)D.

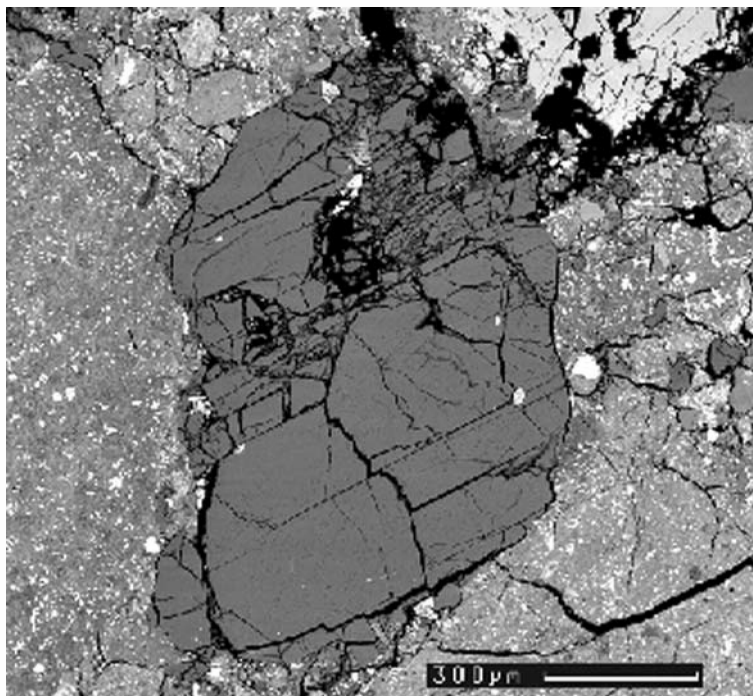


Fig. 5. Backscattered electron image of Kaidun fragment #d(4)A. The fragment is composed largely of a single crystal of albite. The elongate light area in upper center is an inclusion of complex composition (see Fig. 6). The small white grains are apatite. The scale bar is 300 μm .

Clast #d4A

Table 3 shows the chemical composition of the components of clast #d4A. Clast #d4A is a single plagioclase crystal with intergrowths. It has an albitic composition and weak chemical zoning, from $\text{Ab}_{89}\text{An}_{5.4}\text{Or}_{7.1}$ at the center to $\text{Ab}_{90.5}\text{An}_{2.4}\text{Or}_{7.1}$ at the edges.

In clast #d4A, apatite is present as fluorapatite. Aenigmatite is present in clast #d4A in two settings—within a multiphase inclusion (aenigmatite 1) and in an intergrowth with a relatively large apatite crystal (aenigmatite 2). The Fe and Mg contents of the mineral vary somewhat in the different positions (Table 3). The formulas are: $\text{Na}_{1.98}(\text{Fe}^{2+}_{4.13}, \text{Mg}_{0.75}, \text{Ca}_{0.08}, \text{Mn}_{0.08})\text{Ti}_{1.00}(\text{Si}_{5.86}, \text{Al}_{0.16})\text{O}_{20}$ and $\text{Na}_{2.07}(\text{Fe}^{2+}_{3.42}, \text{Mg}_{1.36}, \text{Ca}_{0.11}, \text{Mn}_{0.06})\text{Ti}_{0.99}(\text{Si}_{5.93}, \text{Al}_{0.12})\text{O}_{20}$, for aenigmatite 1 and 2, respectively. The Mg and Mn contents of aenigmatites from clast #d4A differ noticeably from those of terrestrial aenigmatites. The content of MgO in terrestrial aenigmatite from alkaline rocks never exceeds 3 wt% and is usually smaller than 1.5 wt% (Mitrofanova and Afanas'eva 1966; Kostyleva-Labuntsova et al. 1978; Jones 1984; Stolz 1986, and many others), while the MgO contents in aenigmatite from the Kaidun clast are 3.6 and 6.8 wt%. The MnO content in terrestrial aenigmatite usually exceeds 1 wt% and quite often exceeds 2 wt%, while the MnO content in Kaidun aenigmatite is 0.5–0.8 wt%.

As noted above, wilkinsonite occurs only as very small grains. For this reason, we were able to obtain only 2 good

analyses, one of a separate grain and one of an exsolution-like inclusion in a grain of aenigmatite. Both compositions are practically identical and can be approximated by the formula $\text{Na}_{1.97}(\text{Fe}^{2+}_{3.59}, \text{Mg}_{0.21}, \text{Mn}_{0.09}, \text{Ca}_{0.05})(\text{Fe}^{3+}_{1.87}, \text{Al}_{0.12}, \text{Ti}_{0.01})\text{Si}_{5.97}\text{O}_{20}$.

Wilkinsonite from the Kaidun clast has noticeably higher MgO and lower MnO in comparison with the only known terrestrial wilkinsonite (MgO <0.1 wt% and MnO >1.0 wt%; Duggan 1990).

Arfvedsonite is MgO-rich and has the formula $(\text{Na}_{1.93}, \text{Ca}_{0.74}, \text{K}_{0.25})(\text{Mg}_{2.41}, \text{Fe}^{2+}_{1.62}, \text{Mn}_{0.08})(\text{Fe}^{3+}_{0.94}, \text{Al}_{0.06})\text{Si}_{8.01}\text{O}_{22}(\text{OH})_{20}$.

The phyllosilicates are characterized by a variable composition and notable phosphorus content. Small inclusions of phosphates in the aenigmatite grain, in phyllosilicates, and in the fractured zone of the albite are characterized by a low analytic sum and by significant Si, Al, Fe, and Mg.

DISCUSSION

Formation of the Clasts

The texture of the main mass of clast #d(3–5)D is finely crystalline to glassy containing skeletal and subangular plagioclase crystals. This texture probably formed by rapid cooling of a melt. The rounded contact between the body of the clast and the inclusion of carbonaceous matrix seen in #d3D clearly indicates that the material of the clast was in

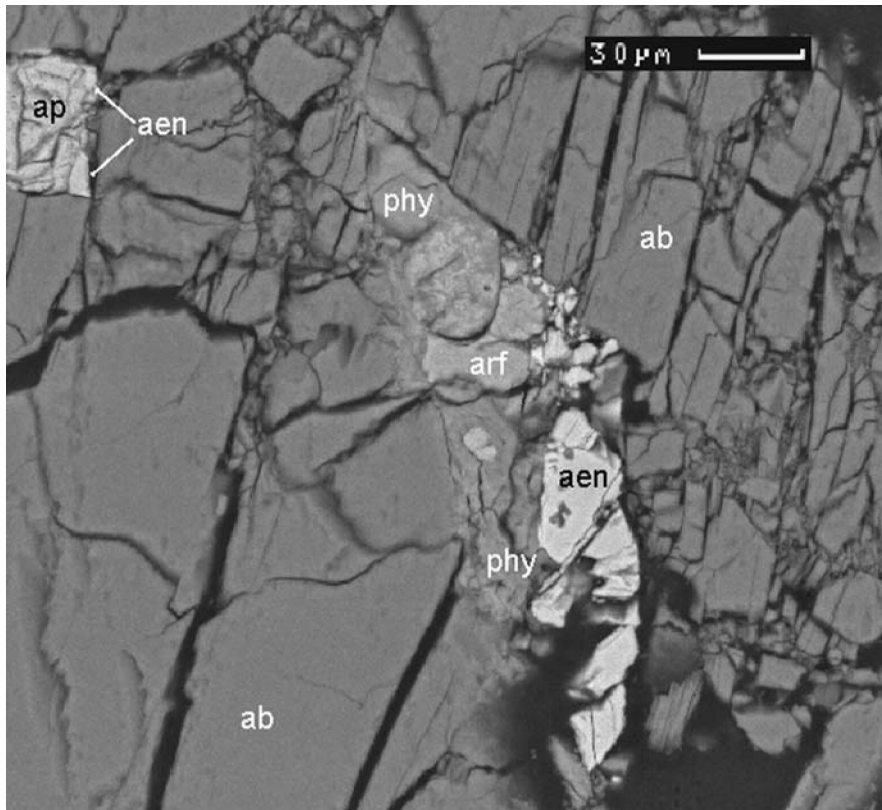


Fig. 6. Backscattered electron image of a part of fragment #d(4)A. At the center is a complex multiphase inclusion containing aenigmatite, wilkinsonite, arfvedsonite, and phyllosilicates. A part of a rather large apatite with 2 small aenigmatite grains at the edges is at the upper left. The chemical compositions of aenigmatite in the multiphase inclusion and the intergrowths with apatite crystal are different (see Table 3). Abbreviations: ab = albite, aen = aenigmatite, arf = arfvedsonite, phy = phyllosilicates. The scale bar is 30 μm .

liquid form during formation of the contact. We suggest that the melt could have interacted with the water-bearing carbonaceous matrix at this time, producing a hydrous melt. The presence of phyllosilicate coatings within voids supports this supposition.

At the same time, the nearly complete lack of sulfur in the matrix and the low iron content (typical components of carbonaceous chondrite matrix) suggests that very little contamination of the melt by the material of the carbonaceous matrix occurred. Interactions were apparently limited primarily to contamination by water and very water-soluble components.

Clearly, the formation of clast #d(3–5)D occurred during a high-velocity impact event. During this event, the material of the impactor was heavily melted. However, the smooth, rounded edges of most of the large mineral grains in clast #d(3–5)D are incompatible with their formation by crystallization of this melt but suggest the opposite process of resorption of crystals in the melt. We suggest that the large mineral grains of the clast are the remains of a previously existing fragment or fragments that have undergone melting.

As the results of experimental studies show (Lofgren

1974, 1980), the shape of plagioclase crystals during crystallization from a melt reflects the degree of supercooling of the melt and its cooling rate. The presence in clast #d(3–5)D of tablet-shaped, skeletal, and subangular crystals of plagioclase suggests that the crystals formed from a rapidly cooling, supercooled melt. High rates of cooling and crystallization are also suggested by the above mentioned high content of foreign ions in the plagioclase and pyroxene of the matrix, as well as the observation that most potassium did not partition into albite during crystallization. According to experimental results (Lofgren 1974, 1980), the level of supercooling ΔT appears to have been $\sim 150^\circ\text{C/hr}$, with a cooling rate of $\sim 5\text{--}10^\circ\text{C/hr}$.

The formation of the clast's voids appears to be related to the presence of a fluid phase and occurred during cooling and crystallization of the melt. This is also supported by the above mentioned cases of plagioclase laths being interrupted by voids, including voids with coated walls. The presence of a fluid phase may be related to contamination by water and other volatiles from the carbonaceous matrix of the meteorite. However, we cannot exclude the possibility of a high volatile content in the primary material of the clast.

The formation of the coatings on the void walls must

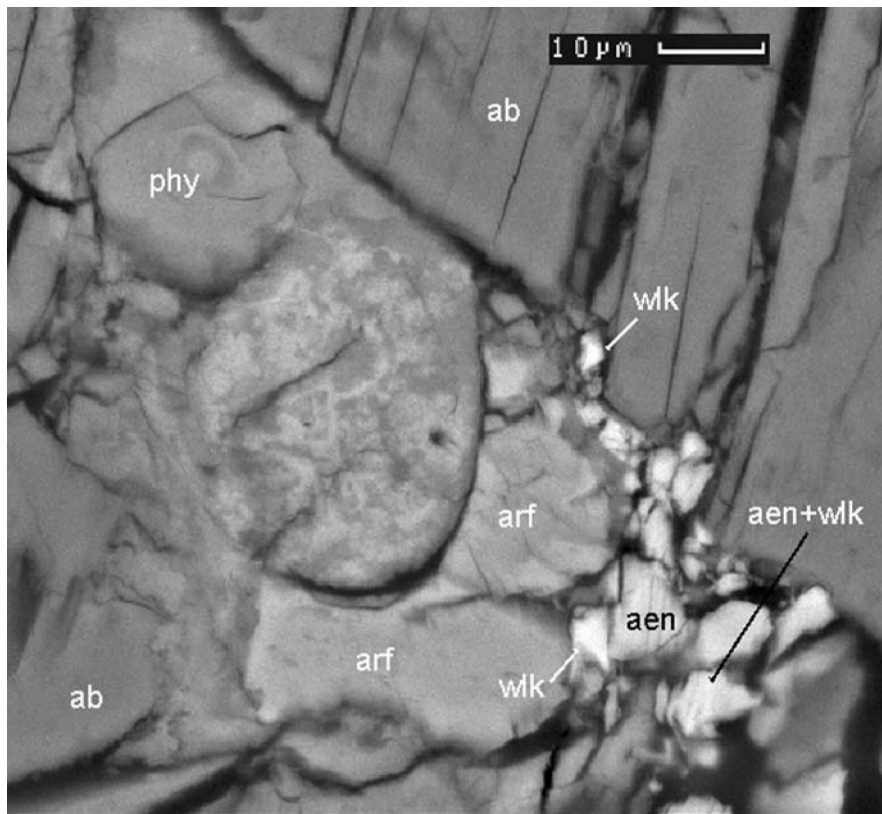


Fig. 7. Backscattered electron image of the wilkinsonite-containing part of the complex inclusion in the #d(4)A fragment. Wilkinsonite of the same composition presents as separate grains and as exsolution-like inclusions in aenigmatite. Abbreviations: wlc = wilkinsonite, others = see caption to Fig. 6. The scale bar is 10 μm .

have occurred during the final stage of formation of the clast, with the formation of the colloform coatings following that of the crystalline coatings.

The composition of the crystalline coatings of the voids of clast #d(3–5)D— $(\text{Mg, Fe, Mn})_5\text{Al}_2\text{O}_8 \cdot n\text{H}_2\text{O}$ —is similar if not identical to the $\text{Mg}_{11}\text{Fe}_4\text{Al}_6\text{O}_{24} \cdot n\text{H}_2\text{O}$ composition of the thin, elongated individual crystals found in the cavities of the chondritic clast #d3A (Ivanov et al. 2000a). We note that no mineral phase of this composition has been observed previously in nature. The formation of crystals of this phase in both cases appears to have occurred from a fluid of identical or extremely similar composition, and most likely they share a single process of formation. The difference in morphology of this phase in clasts #d3A and #d(3–5)D—elongated individual crystals in the first case and a finely crystalline brush in the second case—could reflect differences in formation temperature. In turn, this appears to suggest that the formation of this phase in clast #d(3–5)D occurred at higher temperature than in clast #d3A. We assume the mineral-forming fluid was formed in clast #d(3–5)D during cooling of the melt. In clast #d3A, this phase may have formed from the same fluid after its further cooling during filtration through meteorite material.

In contrast to the previous clast (#d[3–5]D), clast #d4A

does not show evidence of significant secondary changes and appears to have retained its original texture from before its incorporation into the Kaidun parent body. As mentioned above, the crystal's fractured zone may be result of an impact event. The hydrated phases present in the clast—phyllosilicates and hydrous phosphates—may be linked to hydrous alteration in the parent body of the meteorite. Note that during this hydrous alteration, the characteristics of the clast—the alkaline character of the clast's components—were preserved.

Chemistry and Origin of the Clasts

The mineral association of clast #d4A—albite, apatite, aenigmatite, wilkinsonite, and arfvedsonite—clearly indicate its alkaline igneous nature. The formation of this clast probably resulted from extreme differentiation of the source material. We must emphasize that arfvedsonite, aenigmatite and wilkinsonite are represented by MgO-rich varieties and that the latter 2 minerals are notably distinct chemically from their terrestrial analogues.

Four alkaline rock clasts were found previously in the LL3–6 chondritic breccia Adzhi-Bogdo (Bischoff et al. 1993). The main minerals of these clasts are K-feldspar and SiO_2 -

Table 1. Chemical composition of the components from the Kaidun clast #d(3-5)D (average and variations, wt%).

Component	SiO ₂	TiO ₂	Al ₂ O ₃	Cr ₂ O ₃	FeO ^a	MnO	MgO	CaO	Na ₂ O	K ₂ O	P ₂ O ₅	Total	En or Ab	Wo or An	Fs or Or
Large grains															
Augite, n ^b = 35	52.2	0.28	0.89	0.92	12.8	0.51	14.6	17.1	0.42	<0.03	-	99.72	42.4	35.8	21.8
	51.7-53.1	0.20-0.39	0.78-1.01	0.80-1.01	12.4-13.4	0.41-0.59	14.0-14.9	16.6-17.9	0.35-0.58				41.4-43.2	35.1-37.1	21.1-22.7
Pigeonite, n = 5	51.8	0.62	0.42	0.20	26.0	0.61	16.1	4.69	0.20	<0.03	-	100.64	46.8	9.8	43.4
	51.5-52.2	0.60-0.64	0.36-0.48	0.18-0.23	25.8-26.2	0.56-0.67	15.5-16.8	4.58-4.75	0.16-0.25				45.7-47.7	9.7-10.0	42.6-44.4
Apatite ^c , n = 12	0.42	-	-	-	0.86	0.13	0.38	53.0	0.74	-	41.3	101.88 ^e	-	-	-
	0.35-0.51				0.76-0.93	0.08-0.18	0.30-0.44	51.6-53.9	0.62-0.89		40.9-41.7				
Matrix materials															
Plagioclase, n = 19	62.6	0.08	23.1	<0.03	0.65	<0.03-0.05	0.34	4.86	8.52	0.22	0.12	100.49	74.5	24.2	1.3
	60.1-64.3	0.03-0.17	21.4-25.9		0.31-1.01		0.09-0.81	3.14-6.75	6.70-9.44	0.10-0.41	0.04-0.27		64.6-82.1	16.0-34.5	0.62-2.5
Pyroxene, n = 6	48.0	1.67	2.69	0.24	23.2	0.91	10.4	10.0	0.91	0.07	1.32	99.41	33.3	23.2	43.5
	46.9-49.0	1.13-2.20	1.45-4.14	0.12-0.40	19.8-27.6	0.67-1.35	8.5-12.8	8.5-11.5	0.66-1.31	0.03-0.11	0.44-2.64		27.9-40.6	19.7-26.7	36.3-53.4
Anorthoclase ^d	66.5	-	20.1	-	0.99	-	1.23	1.71	8.53	1.88	-	100.94	79.6	8.8	11.6
Matrix ^e , n = 136	58.1	0.53	16.9	0.06	6.89	0.19	2.89	4.55	7.41	0.49	0.92	98.93	-	-	-
	57.7-60.9	0.21-0.75	14.7-21.2	<0.03-0.24	3.00-8.77	0.09-0.32	0.98-7.86	3.22-6.22	5.88-8.29	0.22-1.41	0.22-1.61				
Bulk composition															
Bulk, calculated	57.9	0.52	16.6	0.07	6.98	0.20	3.08	4.86	7.28	0.48	0.98	98.95	-	-	-

^aAll Fe as FeO.^bn = number of analyses.^cApatite contains also F 3.10, Cl 1.95 wt%.^dRepresentative analysis.^eDefocused electron beam 50 × 50 μm.

Table 2. Chemical composition of the cavity coatings from the Kaidun clast #d(3-5)D (average and variations, wt%).

Component	SiO ₂	Al ₂ O ₃	FeO ^a	MnO	MgO	CaO	Na ₂ O	K ₂ O	P ₂ O ₅	S	Total
Colloform coating 1, n ^b = 4	41.9	6.78	15.1	0.24	22.7	0.18	0.59	0.21	<0.03	0.13	87.83
	39.9-43.3	6.51-7.09	14.6-15.8	0.22-0.26	22.2-23.2	0.16-0.19	0.50-0.71	0.20-0.22		0.11-0.13	
Colloform coating 2, n = 5	42.5	12.0	8.80	0.50	25.8	0.16	0.38	0.31	<0.03	0.07	90.52
	41.1-43.5	11.6-12.4	7.96-9.40	0.40-0.59	25.4-26.8	0.12-0.21	0.33-0.45	0.28-0.36		0.05-0.11	
Crystalline coating 1 ^c	6.05	19.1	23.2	0.16	25.0	0.06	0.05	<0.03	0.04	0.09	73.75
Crystalline coating 2 ^c	8.93	19.5	21.4	0.17	29.5	0.04	0.07	<0.03	0.05	0.17	79.83
Crystalline coating 3 ^c	8.71	22.4	22.6	0.20	28.8	0.08	0.05	<0.03	0.10	0.15	83.09
Crystalline coating 1 ^d	-	29.2	35.2	0.18	35.4	-	-	-	-	-	100
Crystalline coating 2 ^d	-	28.7	31.0	0.16	40.1	-	-	-	-	-	100
Crystalline coating 3 ^d	-	30.0	32.0	0.20	37.8	-	-	-	-	-	100

^aAll Fe as FeO. TiO₂ and Cr₂O₃ contents below 0.03 wt%.^bn = number of analyses.^cReal analyses.^dThe same analyses as previous after subtraction of collomorf coating material, normalized to 100%.

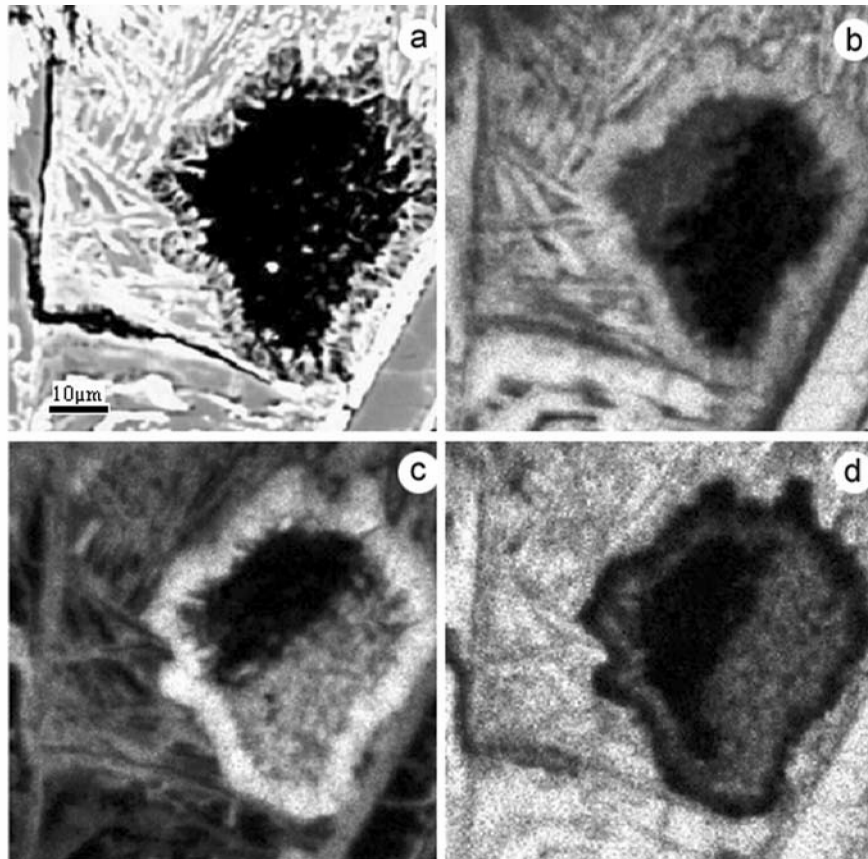


Fig. 8. Backscattered electron image of fragment #d(3–5)D, section #d3D (a) and corresponding X-ray maps Al K_{α} (b), Mg K_{α} (c), and Si K_{α} (d) of the void covered with a crystalline coating. The coating is enriched in Al and Mg and does not contain Si, which is present only on the surface of the crystals as a component of the colloform coating. The scale bar is 10 μm .

phases (tridymite and quartz). The minor phases include albite, chlorapatite, whitlockite, ilmenite, zircon, Ca-poor pyroxene, and a poorly characterized Na, Ti-bearing silicate ($[\text{Na}, \text{Ca}]_{2.7}[\text{Fe}, \text{Mg}]_6\text{Ti}_{1.3}\text{Si}_7\text{O}_{24}$). The sizes of the quartz and K-feldspar grains are up to 700 μm . These clasts were classified as alkali-granitoids. Besides the alkali-granitoid clasts, Adzhi-Bogdo also contains pyroxene-rich clasts containing both Ca-poor and high-Ca pyroxenes. Judging from the similarities of the minor phase compositions, granitoids and pyroxene-rich clasts are related (Bischoff et al. 1993).

We emphasize the significant similarities of the composition of aenigmatite 1 from Kaidun #d4A (Table 3) and of the unidentified Na, Ti-bearing silicate from alkali-granitoid clasts of Adzhi-Bogdo (42.1 wt% SiO_2 , 10.1 TiO_2 , 0.26 Al_2O_3 , 35.5 FeO , 0.24 MnO , 3.7 MgO , 0.27 CaO , 8.2 Na_2O ; Bischoff et al. 1993). The SiO_2 , FeO , and MgO contents are similar in both phases, although, Na_2O shows a marked difference. Na_2O content in the Na, Ti-bearing silicate of Adzhi-Bogdo is possibly overestimated, particularly if albite was used as the Na standard during microprobe analysis and if measurements of both standard and sample were made under standard conditions. Sodium is very unstable under electron beam in albite but very stable in aenigmatite. The use

of the data without additional correction could result in an overestimated sodium content in aenigmatite. If we assign the Na_2O content of the aenigmatite 1 Kaidun #d4A (7.3 wt%) to the Na, Ti-bearing silicate in Adzhi-Bogdo, the formula of the silicate will correspond to aenigmatite and can be written as $\text{Na}_{1.98}(\text{Fe}^{2+}_{4.16}, \text{Mg}_{0.77}, \text{Ca}_{0.04}, \text{Mn}_{0.03})\text{Ti}_{1.06}(\text{Si}_{5.90}, \text{Al}_{0.04})\text{O}_{20}$.

Kaidun clast #d4A and the alkali-granitoid clasts of Adzhi-Bogdo are the only alkaline rock clasts found in meteorites to date. The mineral compositions of these clasts in both meteorites are considerably different. However, the Kaidun clast #d4A is a single large albite crystal with inclusions of other minerals. Kaidun #d4A is evidently a fragment of an alkaline rock and is more coarse-grained compared to the parent rock of granitoid clasts in Adzhi-Bogdo. The composition of the parent rock of Kaidun #d4A is unknown. However, the presence of compositionally similar aenigmatite in both Kaidun #d4A and granitoid clasts of Adzhi-Bogdo (or, in Adzhi-Bogdo, a similar mineral phase) suggests a genetic relationship.

The matrix of clast #d(3–5)D, as mentioned above, has probably been insignificantly contaminated by material from the matrix of the meteorite. This allows us to evaluate the character of the primary material that underwent melting.

Table 3. Chemical composition of the components from the Kaidun clast #d4A (average and variations, wt%).

Component	SiO ₂	TiO ₂	Al ₂ O ₃	Cr ₂ O ₃	FeO ^a	MnO	MgO	CaO	Na ₂ O	K ₂ O	P ₂ O ₅	Total
Albite, n ^b = 8	67.9	—	19.4	—	0.17	<0.03	<0.03–0.08	0.60	10.4	1.19	—	99.66
	67.1–69.2	—	18.9–19.9	—	0.09–0.27	—	—	0.50–0.70	10.1–10.8	1.11–1.29	—	—
Apatite, * n = 3	0.62	—	—	—	0.60	0.14	0.18	53.5	0.19	—	40.7	99.77 ^c
	0.46–0.70	—	—	—	0.49–0.73	0.10–0.17	0.10–0.30	53.2–53.8	0.12–0.23	—	39.5–41.3	—
Aenigmatite 1, n = 6	42.1	9.58	0.98	<0.03–0.11	35.4	0.68	3.64	0.52	7.32	<0.03	0.20	100.42
	41.5–42.5	8.83–10.2	0.77–1.36	—	34.1–36.4	0.59–0.78	3.49–3.75	0.44–0.58	6.92–7.58	—	0.12–0.27	—
Aenigmatite 2, n = 2	44.1	9.78	0.76	<0.03	30.4	0.52	6.81	0.76	7.96	<0.03	0.47	101.56
Wilkinsonite ^d	42.2	0.08	0.76	<0.03	46.2	0.76	0.96	0.39	7.58	0.05	—	98.98
Wilkinsonite ^e	42.6	0.20	0.64	<0.03	46.6	0.70	1.04	0.28	7.72	<0.03	—	99.78
Arvedsonite, n = 4	53.5	<0.03–0.04	0.33	<0.03	20.4	0.63	10.8	4.59	6.63	1.37	—	98.25
	52.6–54.2	—	0.24–0.38	—	20.3–20.6	0.50–0.71	10.5–11.0	4.06–5.10	6.39–6.88	1.36–1.38	—	—
Phyllosilicate ^f	47.2	<0.03	6.39	—	17.0	1.33	13.9	1.43	0.16	0.42	1.16	88.99
Phyllosilicate ^f	38.5	<0.03	7.30	—	14.2	0.37	21.7	0.39	0.64	0.21	0.33	83.64

^aAll Fe as FeO.^bn = number of analyses.^cApatite contains also F 3.33, Cl 0.51 wt%.^dSeparate grain.^eInclusion in aenigmatite.^fSelected analyses.

When determining the nature of the melted primary material, the key parameters appear to be: 1) relict character of the large grains of the clast under study—two different pyroxenes and apatite; 2) the high content of alkali plagioclase in the clast; and 3) the lack of significant amounts of olivine. These parameters indicate a strongly differentiated character for the melted material. Based on the bulk SiO₂ content and the sum of Na₂O + K₂O in clast #d(3–5)D, in reference to earthlike rocks, the clast falls among the intermediate rocks of the subalkaline series, in the family of trachyandesites (Bogatikov et al. 1981).

The clasts in this investigation show many similar mineralogical characteristics: albitic or nearly albitic plagioclase compositions and the presence of fluorapatite. The evidence suggests that both clasts are genetically related and formed from the same parent body. However, the great difference in the textures of the clasts (intensive remelting of clast #d(3–5)D and primary igneous character of clast #d4A) suggests that these clasts were incorporated into the Kaidun parent body during different impact events.

Among achondrites, the eucrites show some affinities to Kaidun clasts (Mittlefehldt et al. 1998; Yamaguchi et al. 1996). These meteorites have essentially pyroxene-plagioclase compositions with little or no olivine. The size of pyroxene grains in eucrites vary within wide boundaries—from tens of μm to 1 mm. The compositions of some eucritic pyroxenes are similar to the large grains of pyroxene in the Kaidun clasts (Yamaguchi et al. 1996). Phosphates in the eucrites are represented by fluorapatite and whitlockite (merrillite), and the size of their grains varies from submicrometers to ~50 μm (Delaney et al. 1984). The size of the plagioclase grains, in some cases, reaches 0.7 mm (Yamaguchi et al. 1996). However, unlike the plagioclase of clast #d(3–5)D, the composition of the plagioclase of the eucrites is strongly calcic (anorthite-bytownite) and is characterized by a very low K₂O content (=0.1 wt%; Mittlefehldt et al. 1998). Thus, it is clear that linking the formation of the Kaidun clasts with eucrite material is not warranted.

Meteorites of the SNC group are of great interest, especially the basaltic shergottites (Stolper and McSween 1979; Stofler et al. 1986; McCoy et al. 1992, 1999; McSween and Treiman 1998; McSween et al. 1996; Meyer 1998; Rubin et al. 2000; Taylor et al. 2000; Zipfel 2000). These meteorites consist of 40–70 vol% of large, often >1 mm, crystals of pigeonite and subcalcic augite with homogeneous cores and strongly zoned peripheries. Shergottite plagioclase commonly occurs in the form of zoned maskelynite with composition varying within broad boundaries: An_{36–68}Ab_{31–63}Or_{1–7}. The maskelynite content in various shergottite samples also varies widely: ~9–48 vol%. Phosphates in shergottites are represented by whitlockite (merrillite) and F-containing chlorapatite. In the shergottite QUE 94201, the apatite crystals have fluorine-rich cores and

chlorine-rich outer layers (McSween et al. 1996). The content of olivine Fa_{40-97} in shergottites, as a rule, does not exceed 10 vol% and in Sayh Al Uhaymir reaches 25 vol% (Zipfel 2000). Some basaltic shergottites (QUE 94201, Zagami) contain different lithologies interlinked by processes of fractional crystallization (McSween et al. 1996; McCoy et al. 1999).

The material of clast #d(3–5)D is similar in some characteristics to the material of the basaltic shergottites. The olivine content of clast #d(3–5)D, according to norm calculations, is less than 5 vol%. The clast contains fairly large grains of augite and pigeonite, which is typical for shergottites. The clast's pyroxene compositions fall in fields corresponding to the pyroxenes of shergottites in the pyroxene prism (Meyer 1998) (Fig. 9). However, the average calcium content in the augite clast is somewhat lower and pigeonite is somewhat higher in comparison with the calcium content of shergottite pyroxenes. This difference may be connected with the lower equilibration temperature of pyroxene clasts in comparison with the equilibration temperature of shergottite pyroxenes (Lindsley 1983). The lack of the zoning, which is characteristic for the pyroxenes of

shergottites in the peripheries of the grains, may be explained by their partial dissolution during melting of the clast, and also by homogenization during heating.

CONCLUSION

Clasts of alkaline (the second find in meteorites) and subalkaline rocks were found in the Kaidun meteorite. Their mineralogical characteristics suggest a mutual genetic relationship and origin from the same parent body. Clast #d4A is a large crystal of albite with inclusions of fluorapatite, arfvedsonite, aenigmatite, and wilkinsonite. The latter two minerals were not previously known in meteorites. Clast #d(3–5)D has a melt crystallization texture of mainly feldspar (oligoclase) composition and contains relict grains of both High-Ca and low-Ca pyroxene plus fluorapatite. The textural and mineralogical characteristics of the clasts suggest an origin by extensive igneous differentiation. Such processes most likely took place in a rather large differentiated body. We note that the material of clast #d(3–5)D is similar in some mineralogical characteristics to the material of the basaltic shergottites.

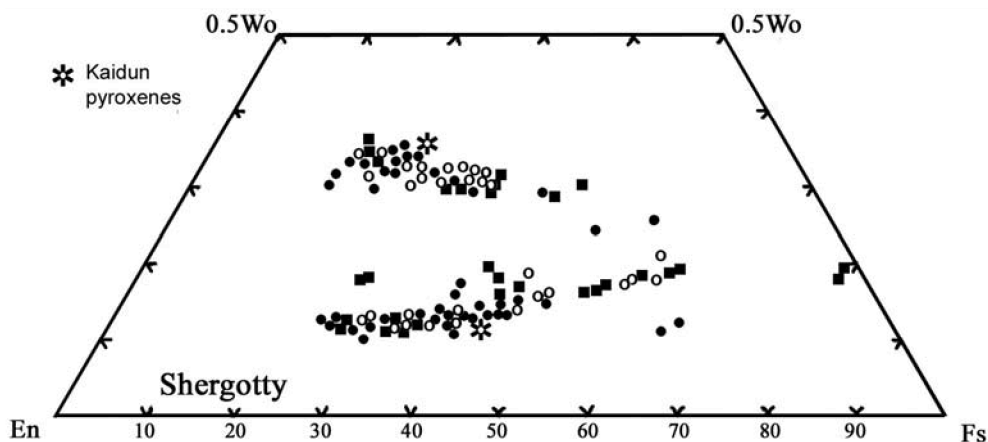


Fig. 9. Pyroxene compositional diagram for the Shergotty meteorite (Meyer 1998) and for large pyroxene grains from the Kaidun #d(3–5)D fragment. The Kaidun pyroxenes, both high-Ca and low-Ca, have rather uniform composition (see Table 1). The Kaidun points are averages of 35 analyses of several augite grains (upper point) and of 5 analyses of one pigeonite grain (lower point).

Acknowledgments—This work was supported by RFBR grant 01–05–64239 to A. V. Ivanov and the NASA Cosmochemistry Program to M. E. Zolensky. We thank A. T. Basilevsky, V. I. Feldman, M. A. Nazarov, and A. A. Yaroshevsky for useful discussion and I. A. Stroganov for assistance in preparation of the manuscript. Reviews by Jack Berkley and an anonymous reviewer, as well as comments of Associate Editor Ed Scott resulted in considerable improvement of the paper.

Editorial Handling—Dr. Edward Scott

REFERENCES

- Bischoff A., Geiger T., Palme H., Spettel B., Schultz L., Scherer P., Schluter J. and Lkhamsuren J. 1993. Mineralogy, chemistry, and noble gas contents of Adzhi-Bogdo—An LL3–6 chondritic breccia with L-chondritic and granitoid clasts. *Meteoritics* 28: 570–578.
- Bogatikov O. A., Gon'shakova V. I., Eframova S. V. et al. 1981. *Classification and nomenclature of magmatic rocks*. Moscow: Nedra Press. 160 p. In Russian.
- Clayton R. N., Mayeda T. K., Ivanov A. V., and MacPherson G. J. 1994. Oxygen isotopes in Kaidun (abstract). 25th Lunar and Planetary Science Conference. pp. 269–270.
- Delaney J. S., O'Neil C., and Prinz M. 1984. Phosphate minerals in

- euclites (abstract). 15th Lunar and Planetary Science Conference. pp. 208–209.
- Duggan M. B. 1990. Wilkinsonite, $\text{Na}_2\text{Fe}^{2+}_4\text{Fe}^{3+}_2\text{Si}_6\text{O}_{20}$, a new member of the aenigmatite group from the Warrumbungle Volcano, New South Wales, Australia. *American Mineralogist* 75:694–701.
- Jones A. P. 1984. Mafic silicates from the nepheline syenites of the Motzfeld centre, South Greenland. *Mineralogical Magazine* 48: 1–12.
- Ivanov A. V. 1989. The Kaidun meteorite: Composition and history. *Geochemistry International* 26:84–91.
- Ivanov A. V., Khisina N. R., Kononkova N. N., and Petushkova L. V. 1988. Iron crystals in the Kaidun meteorite: Process of new type? (abstract). 19th Lunar and Planetary Science Conference. pp. 529–530.
- Ivanov A. V., MacPherson G. J., Zolensky M. E., Kononkova N. N., and Migdisova L. F. 1996. The Kaidun meteorite: Composition and origin of inclusions in the metal of the enstatite chondrite clast. *Meteoritics & Planetary Science* 31:621–626.
- Ivanov A. V., Kurat G., Migdisova L. F., Brandstaetter F., and Kononkova N. N. 1998. The Kaidun meteorite: Pre- and postaccretionary aqueous alterations of metal in an enstatite chondrite fragment. *Geochemistry International* 36:101–106.
- Ivanov A. V., Zolensky M. E., and Yang S. V. 2000a. The Kaidun meteorite: Evidence for aqueous alteration and precipitation (abstract). *Meteoritics & Planetary Science* 35:A82.
- Ivanov A. V., Zolensky M. E., Saito A., Ohsumi K., Yang S. V., Kononkova N. N., and Mikouchi T. 2000b. Florenskyite, FeTiP , a new phosphide from the Kaidun meteorite. *American Mineralogist* 85:1082–1086.
- Kostyleva-Labuntsova E. E., Borutskaya B. E., Sokolova M. N., Shlyukova Z. V., Dorfman M. D., and Dudkin O. B. 1978. *Mineralogy of the Khibin massiv*. Vol. 2. Moscow: Nauka Press. In Russian.
- Lindsley D. H. 1983. Pyroxene thermometry. *American Mineralogist* 68:477–493.
- Lofgren G. 1974. An experimental study of plagioclase crystal morphology: Isothermal crystallization. *American Journal of Science* 274:243–273.
- Lofgren G. 1980. Experimental studies on the dynamic crystallization of silicate melt. In *Physics of magmatic processes*, edited by Hargraves R. B. Princeton: Princeton University Press. pp. 487–551.
- Meyer C. 1998. *Mars meteorite compendium*. Houston: NASA Johnson Space Center. 237 p.
- McCoy T. J., Taylor G. J., and Keil K. 1992. Zagami: Product of a two-stage magmatic history. *Geochimica et Cosmochimica Acta* 56:3571–3582.
- McCoy T. J., Wadhwa M. and Keil K. 1999. New lithologies in the Zagami meteorite: Evidence for fractional crystallization of a single magm unit on Mars. *Geochimica et Cosmochimica Acta* 63:1249–1262.
- McSween H. Y., Jr. and Treiman A. H. 1998. Martian meteorites. In *Planetary materials*, edited by Papike J. J. *Reviews in Mineralogy* 36:6-01–6-53.
- McSween H. Y., Jr., Eisenhour D. D., Taylor L. A., Wadhwa M., and Crozaz G. 1996. QUE 94201 shergottite: Crystallization of a Martian basaltic magma. *Geochimica et Cosmochimica Acta* 60: 4563–4569.
- Mitrofanova F. L. and Afanas'eva L. I. 1966. Aenigmatite from the alkali syenites of the Eastern Sayan mountains. *Doklady Akademii Nauk* 166:444. In Russian.
- Mittlefehldt D. W., McCoy T. J., Goodrich C. A., and Kracher A. 1998. Non-chondritic meteorites from asteroidal bodies. In *Planetary materials*, edited by Papike J. J. *Reviews in Mineralogy* 36:4-01–4-195.
- Rubin A. E., Warren P. H., Greenwood J. P., Verish R. S., Leshin L. A., and Hervig R. L. 2000. Petrology of Los Angeles: A new basaltic shergottite find (abstract #1963). 31st Lunar and Planetary Science Conference. CD-ROM.
- Stoffler D., Ostertag R., Jammes C., Pfannschmidt G., Sen Gupta P. R., Simon S. B., Papike J. J., and Beauchamp R. H. 1986. Shock metamorphism and petrography of the Shergotty achondrite. *Geochimica et Cosmochimica Acta* 50:889–903.
- Stolper E. and McSween H. Y., Jr. 1979. Petrology and origin of the shergottite meteorites. *Geochimica et Cosmochimica Acta* 43: 1475–1498.
- Stolz A. J. 1986. Mineralogy of the Nandewer Volcano, northeastern